Imaging the Conductance of Integer and Fractional Quantum Hall Edge States

Nikola Pascher,* Clemens Rössler, Thomas Ihn, Klaus Ensslin, Christian Reichl, and Werner Wegscheider

Solid State Physics Laboratory, ETH Zurich, 8093 Zurich, Switzerland

(Received 19 September 2013; published 30 January 2014)

We measure the conductance of a quantum point contact while the biased tip of a scanning probe microscope induces a depleted region in the electron gas underneath. At a finite magnetic field, we find plateaus in the real-space maps of the conductance as a function of tip position at integer ($\nu = 1, 2, 3, 4, 6, 8$) and fractional ($\nu = 1/3, 2/3, 5/3, 4/5$) values of transmission. They resemble theoretically predicted compressible and incompressible stripes of quantum Hall edge states. The scanning tip allows us to shift the constriction limiting the conductance in real space over distances of many microns. The resulting stripes of integer and fractional filling factors are rugged on scales of a few hundred nanometers, i.e., on a scale much smaller than the zero-field elastic mean free path of the electrons. Our experiments demonstrate that microscopic inhomogeneities are relevant even in high-quality samples and lead to locally strongly fluctuating widths of incompressible regions even down to their complete suppression for certain tip positions. The macroscopic quantization of the Hall resistance measured experimentally in a nonlocal contact configuration survives in the presence of these inhomogeneities, and the relevant local energy scale for the $\nu = 2$ state turns out to be independent of tip position.

DOI: 10.1103/PhysRevX.4.011014 Subject Areas: Nanophysics, Strongly Correlated Materials

I. INTRODUCTION

Two-dimensional electron gases at high magnetic fields applied normal to the electron-gas plane exhibit the quantum Hall effect. The integer [1] and fractional [2] quantum Hall effects are two different macroscopic quantum phenomena, which lead to surprisingly similar observations in electron transport experiments. The similar phenomenology of both effects is commonly believed to be a result of one-dimensional channels at the sample edges, which transmit electrical signals without losses between contacts separated by macroscopic distances [3–5].

In the integer quantum Hall effect, each occupied bulk Landau level gives rise to a pair of counterpropagating channels at opposite sample edges [3,4]. Each counterpropagating pair contributes one conductance quantum e^2/h to the total conductance of the quantum Hall fluid, giving a total quantized conductance (Hall conductance) of $e^2/h \times \nu$, where the integer filling factor ν is the number of spin-resolved Landau levels occupied in the bulk [4,6]. Spin degeneracy of edge channels can be lifted by Zeeman splitting enhanced by exchange interaction effects leading to a spatial substructure [7,8]. Edge channels in the fractional quantum Hall effect have been theoretically proposed [9–13]. Exchange and correlation effects can bring about a spatial substructure beyond the spin splitting of Landau levels, an effect called edge reconstruction [14–16]. Concerning transport, however, theory predicts the same form of the quantized conductance as in the integer regime, but with fractional values of ν, in agreement with the experiment [2].

Early experiments showed spatially resolved edge-channel transport with various techniques [17–19]. Alternative local investigations of the integer quantum Hall effect employed scanning probe techniques, such as scanned potential microscopy [20], the scanning single electron transistor [21], or subsurface charge accumulation imaging [22]. Local gate electrodes enable selective backscattering experiments of integer [23] or fractional [24,25] quantum Hall edge channels. Similarly, narrow quantum point contact (QPC) constrictions allow experimentalists to control local scattering between counterpropagating integer [26,27] or fractional edge channels [28–30]. Scanning gate microscopy (SGM) experiments on quantum point contacts in the integer quantum Hall regime have complemented the conventional transport experiments by inducing a local potential perturbation in the electron gas near the quantum point contact with the scanning tip [31,32]. This arrangement leads to tip-controlled spatially resolved selective backscattering of integer edge channels. Most recently, an experiment by Paradiso and co-workers [32] focused on exploring the physics of fractional quantum Hall edge states. The experiment found evidence for the transmission and backscattering of fractional edge channels through a constriction by a statistical analysis of scanning gate images, taken at a temperature of 250 mK.

*npascher@phys.ethz.ch

In this paper, we report scanning gate experiments at an electron temperature of 170 mK that explore the formation of integer and fractional quantum Hall edge channels in a constriction under the influence of a scanning tip. Our measurements exhibit fractional transmission in the raw data without a statistical analysis. We find an unprecedented rich structure on the local scale, which we interpret as an interplay between the interaction-driven local formation of correlated states leading to edge reconstruction and small residual potential variations occurring in our high-mobility sample on typical length scales of a few hundred nanometers, far below the zero-field elastic mean free path of electrons.

II. OBSERVATION OF QUANTUM HALL STATES

Nanostructures are patterned on top of a high-mobility GaAs-AlGaAs heterostructure wafer with a two-dimensional electron gas (2DEG) forming 120 nm below the surface. The 2DEG has a density of 1.9×10^{11} cm^{-2} and a mobility of 3.5×10^{6} cm^2/Vs. The 2DEG is etched in the shape of a Hall bar, and Ohmic contacts are deposited. All quantities that are schematically summarized in Fig. 1(a) are measured as a function of tip position. The results are obtained with a QPC, where the minimal distance between the two gates is 800 nm. During the experiments, the QPC gates are biased at a voltage of −0.5 V, which is enough to deplete the underlying electron gas and define a narrow channel [33]. An ac bias voltage of $V_{\mathrm{SD,ac}} = 20\ \mu$V is applied, and the modulated source-drain current I_{SD} is measured simultaneously with standard lock-in techniques [see Fig. 1(a)]. This bias voltage is chosen experimentally such that features do not get broadened. By simultaneously measuring the source-drain current I_{SD} and the diagonal voltage V_D, we determine $G = \frac{I_{\mathrm{SD}}}{V_D} = \frac{e^2}{h}\nu_{\mathrm{QPC}}$ and therefore the number of transmitted QPC modes ν_{QPC} [6]. The measurements are carried out at an electron temperature of 170 mK in a quantizing magnetic field B perpendicular to the 2DEG plane.

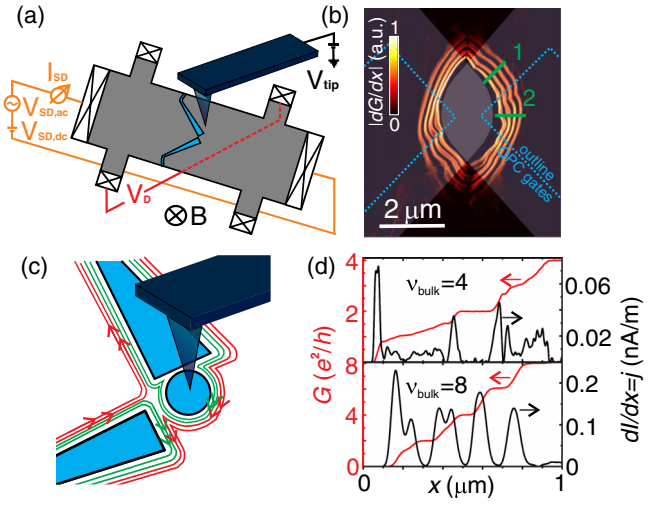

FIG. 1 (color online). (a) Schematics of the experimental setup. All indicated parameters are recorded as a function of tip position. The QPC top gates are highlighted in blue. The QPC forms at the minimum separation of the two gates, which is 800 nm. (b) Typical differential conductance map measured at a bulk filling factor of $\nu_{\mathrm{bulk}} = 8$, corresponding to an external magnetic field of 1 T. The general shape of the observed feature can be understood as an electrostatic fingerprint of the depletion zones of the gates, as highlighted with the white shaded areas. (c) Blow-up of the region around the QPC in (a). The tip is used to selectively backscatter edge channels. In the sketch shown here, two spin-degenerate edge channels are reflected and two are transmitted; thus, the registered conductance will be $4e^2/h$. (d) Line cuts at the position of the green line number 2 for filling factors $\nu_{\mathrm{bulk}} = 4$ and 8 and their numerical derivative with respect to tip position. The conductance changes in steps of e^2/h as a function of tip position, depending on how many edge channels get transmitted or reflected. Even filling factors appear as distinct plateaus, odd filling factors as shoulders.

In the SGM experiment, the voltage-biased tip of the microscope is used to induce a local potential perturbation in the 2DEG [34]. A constant voltage of $V_{\mathrm{tip}} = -4.5$ V is applied to the tip so that the electron gas underneath it gets totally depleted, leading to a disk-shaped region of zero electron density with a radius of about 1.2 μm. This value is estimated from the diameter of the region of total depletion in the typical lens-shaped feature that is observed for all filling factors. The tip consists of a focused-ion-beam-sharpened platinum-iridium wire (radius about 20 nm).

In Fig 1(b) we show a typical SGM picture, measured at a bulk filling factor $\nu_{\mathrm{bulk}} = 8$, corresponding to a magnetic field $B = 1$ T. The colors encode the values of the derivative of the conductance with respect to the x direction. The blue dashed lines show the outline of the metallic gate fingers defining the QPC. The general shape of the rich pattern is mainly caused by electrostatics. We indicate a fingerprint of the shape of the depletion zones along the gate edges, as shown by the gray shading. The width between the central lens and the outer contour of the bright region is roughly given by the width of the QPC. The fine structure deserves a more-detailed discussion. As illustrated in Fig. 1(c), applying a sufficiently negative voltage to the tip leads to a disk-shaped region of total depletion underneath it. When this tip-depleted region comes close to the QPC gap, it consecutively reflects edge channels [see Fig. 1(c)] until it leads to total depletion of the electron gas in the narrow QPC channel [35]. With the filling factor in the bulk being adjusted to 8, as is the case for Fig. 1(b), not accounting for spin splitting, four spin-degenerate even-integer edge channels are present. Once the tip approaches the QPC, the two depletion regions of the tip and the negatively biased gates are so close to each other that the innermost edge channels are reflected and the outer edge channels are still transmitted. Consequently, the detected QPC conductance $G = \frac{e^2}{h}\nu_{\mathrm{QPC}}$ is decreased in steps. In the following, we drop the distinction between ν_{bulk} and ν_{QPC}. We always address the local filling factor

ν_{QPC} unless stated otherwise. Figure 1(d) shows line cuts at the position of green line number 2 in Fig. 1(b) for filling factors $\nu_{\mathrm{bulk}} = 4$ and 8 and their numerical derivatives with respect to tip position. If the tip is far away from the QPC constriction, we measure the bulk filling factor. If it approaches the QPC gap, edge channels are reflected one after the other, leading to stepwise-reduced conductance values. The even filling factors are seen as very pronounced plateaus, the odd filling factors are less clearly seen. This is a manifestation of the relative magnitude of the energy gaps dominating transport: Because the separation of Landau levels $\hbar\omega_c$ is by orders of magnitude larger than the energy scale for spin splitting $g\mu_B B$ (Zeeman gap) the respective plateaus are more or less pronounced, respectively. Plateaus in the conductance as a function of tip position correspond to the length scale where the system can compensate for a change in the electrostatic potential without changing the filling factor in the QPC. Thus, one might assume that the width of the plateaus as measured with SGM is related to the width of the incompressible region in the center of the QPC [5,9,31,32,36,37]. Roughly speaking, the first derivative of the measured source-drain current with respect to the tip position corresponds to the current density that flows in the respective edge channel $dI/dx = j(x)$ [38]. The images show that the change of current with position (current density tentatively defined with the above-mentioned relation) is high in between the plateaus and zero at the position of the plateaus. This increase of dI/dx is due to the formation of an incompressible stripe (in the spirit of Chklovskii *et al.* [5]) in the center of the constriction that supports the additional current [39,40]. At higher magnetic fields, significantly more fine structure of compressible and incompressible stripes can be resolved [Fig. 1(d)]. The current density is especially high at the edge of the compressible stripe. The complicated structure inside the compressible stripe at a bulk filling factor of 4 might support the idea that the edge channels are reconstructed to consist of a fine structure of different integer and fractional contributions [40].

Figure 2 shows a series of images taken at magnetic-field values of 2, 3.5, and 8 T, corresponding to bulk filling factors of 4, 2, and 1. In all images, the plateaus corresponding to even-integer filling factors show up as pronounced dark rings. Odd-integer filling factors can be observed as thinner rings, as the corresponding plateaus are less pronounced. The maximum number of resolvable integer plateaus corresponds to the filling factor that was adjusted in the bulk. The higher the magnetic field, the more fine structure can be resolved between integer filling factors. At a bulk filling factor of 2, a pronounced ring with the spin-polarized filling factor 1 can be measured. At a magnetic field of 8 T, where the bulk filling factor is 1, the fine structure is very rich. There are two plateaus of constant fractional filling factor, $\nu = 1/3$ and $2/3$, going all around the lens.

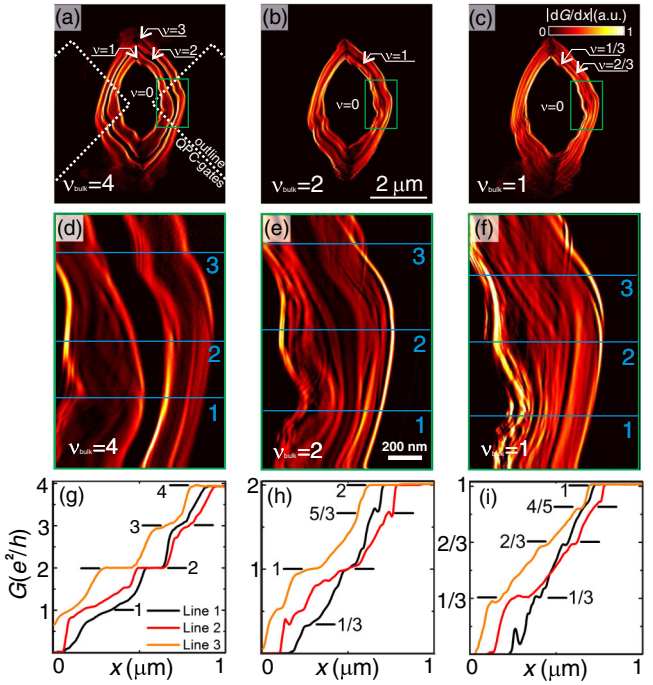

FIG. 2 (color online). (a)–(c) Conductance maps at bulk filling factors 4, 2, and 1, corresponding to magnetic-field values of 2, 3.5, and 8 T. Even filling factors can be seen as very pronounced rings of constant conductance. Odd filling factors show up as shoulders. (d)–(f) High resolution zooms taken at the position of the green frames in (a)–(c). (d) Bulk filling factor of 4. The $\nu = 2$ plateau is clearly resolved, $\nu = 1$ and $\nu = 3$ appear as shoulders. (e) Bulk filling factor of 2. (f) Bulk filling factor of 1. Panels (g)–(i) show line cuts at the positions of the blue lines. Even, odd, and fractional filling factors can be resolved.

In order to characterize the fine structure between integer plateaus, Figs. 2(d)–2(f) show close-ups with high spatial resolution at the position of the green frames in Figs. 2(a)–2(c). With the help of the line cuts [Figs. 2(g)–2(i)] at the positions of the blue lines, most of the fine features can be assigned to quantum Hall plateaus. Others might more likely be caused by disorder-induced antidot or quantum-dot resonances [41–44]. They can be distinguished by comparing the stability and appearance in real space of the two effects. Disorder-induced resonances show up as ringlike features with spacing of the order of 10 nm. If stripes of suppressed dG/dx can be seen that are stable on length scales of 1 order of magnitude larger and that exhibit the right value of the integer or fractional conductance, they are assigned to be quantum Hall induced. At a bulk filling factor of 4 [Figs. 2(d)–2(g)], even and odd filling factors show up as clear plateaus. For a bulk filling factor of 2 [Figs. 2(e) and 2(h)], we see a clear stripe for the $\nu = 1$ plateau. Again, the structure is very rich. More features show up at fractional values of e^2/h, e.g., $1/3$ and $5/3$. When the filling factor in the bulk is 1 [Figs. 2(f) and 2(i)], we see very clear indications for fractional states. There are some regions where the conductance displays a clear

plateau. This allows us to resolve the fractional states with conductance $1/3$, $2/3$, and $4/5$, which can also be observed in conventional transport experiments [45]. These findings show that, by placing the tip at different positions, the potential landscape of the QPC can be modified in a way that it is more favorable to transmit fractional edge channels. If this is the case, plateaus with fractional filling factors are resolved. From these images, we can draw conclusions about the edge and its roughness. Along the edge, the structure is irregular on a length scale of a few hundred nanometers, indicating edge roughness on this scale. The conductance maps also show a lot of fine structure in between the plateaus. This is an indication that conductance at the edge is provided by a fine fabric of different conductance paths [40].

III. POSITION INDEPENDENCE OF THE $\nu = 2$ ENERGY GAP

SGM offers the possibility to investigate the quantum Hall energy gaps with spatial resolution by applying a finite dc source-drain bias voltage $V_{\mathrm{SD,dc}}$. For these measurements, a small ac modulation of 50 μV is applied to the tip so that the transconductance with respect to the tip can be measured. Then, line number 1 in Fig 1(b) is repeatedly scanned, while after each line, $V_{\mathrm{SD,dc}}$ is changed. This kind of measurement is performed for three different magnetic-field values, corresponding to the bulk filling factors 8, 6, and 4. The derivative with respect to the gate voltage [Fig. 3(b)] is calculated numerically. The results are depicted in Fig. 3(a), together with similar transconductance results obtained in conventional transport experiments [Fig. 3(b)]. Different magnetic-field values are applied in Figs. 3(a) and 3(b) to compensate for a slightly changed electron density in two different cooldown cycles. The very broad even-filling-factor plateaus give rise to very clear diamonds, odd filling factors are less pronounced, and fractional states cannot be clearly resolved in these measurements [33].

In an elementary single-particle description [6,46], the size of the energy gaps for the even-numbered filling factors is read from the finite-bias diamonds [see Fig. 3(a), dashed lines]. The extracted gaps correspond to the expected values, which can be calculated according to $\Delta E = \hbar\omega_c$. The finite-bias measurements in Figs. 3(a) and 3(b) are rather different in their details. The reason lies in the fact that in Fig. 3(a), we look at a QPC that is formed between the tip and the left gate, whereas in Fig. 3(b), we measure the QPC formed between the two gates. Furthermore, the two measurements were made in two different cooldowns.

Spatial resolution is not a limit for resolving the energy gaps for fractional and odd filling factors. The relevant parameter in this case is temperature. This can be understood nicely by comparing the conventional transport experiments [Fig. 3(b)] and the data obtained with SGM [Fig. 3(a)]. If spatial resolution is the limiting parameter, the odd filling factors should be especially clearly resolvable in conventional transport.

The irregularity of the structures in Fig. 2 is attributed to edge roughness, which is accompanied by a complicated and irregular local electrostatic landscape. Yet one could imagine that, because of different local properties of the 2DEG, the local energy gaps could also be different. To check this, different lines across the ring-shaped feature are examined [as shown in Fig. 4(a)], and the values obtained for the energy gaps, as they can be read from Fig. 4(b) for filling factor 2, are compared. The energy gaps are found to be position independent and have the expected value of

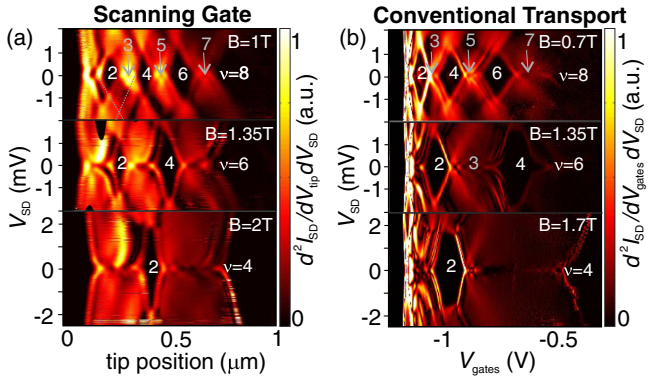

FIG. 3 (color online). False color plots of the transconductance $dI^2_{\mathrm{SD}}/dV_{\mathrm{tip}}dV_{\mathrm{SD}}$ or $dI^2_{\mathrm{SD}}/dV_{\mathrm{gates}}dV_{\mathrm{SD}}$. The derivative with respect to the tip is measured directly by putting a small ac modulation on the tip. The derivative with respect to the voltage on the gates V_{gates} in (b) is calculated numerically. Regions of even filling factors appear as black diamonds centered around $V_{\mathrm{SD}} = 0$ mV. The dashed lines in (a) are guides to the eye to show how we determine the size of the energy gap. The two data sets are taken in different cooldowns.

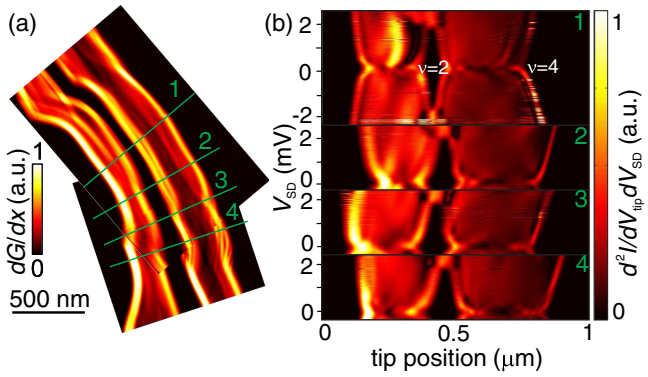

FIG. 4 (color online). (a) Close-up of the feature close to line number 1 in Fig. 1(b). The structures are rugged on a scale of several 100 nm. To examine the position dependence of the energy gaps, line scans were taken along lines 1–4. (b) The values for the energy gaps can be deduced from the closing point of the black diamonds. They are the same for every line; thus, the energy gaps are not position dependent, despite the irregularity of the observed feature.

3.4 ± 0.05 meV at $B = 2$ T, in agreement with the cyclotron energy at this magnetic field.

IV. SIMULATIONS

Paradiso *et al.* measured the width of a conducting stripe in scanning gate images and identified this with the compressible edge-state region in the potential landscape [32,35]. In order to obtain the width of compressible and incompressible regions in real space, one needs to carefully consider the gate as well as tip-induced potentials, which are known only with limited accuracy. We start from a simple model capturing the essentials of the involved potentials and then calculate the regions of constant conductance in scanning gate images.

We perform calculations using the saddle-point model in a magnetic field by Fertig and Halperin [48,49] (FH model), where electron-electron interactions are neglected. We compare the results with the model by Chklovskii, Matveev, and Shklovskii (CMS model), where electron-electron interactions are taken into account [47]. For both methods, the potential landscape of the QPC as influenced by the scanned tip is approximated as a superposition of a saddle-point potential (QPC) [49] and a Lorentzian potential (tip) [34]:

$$V_{\mathrm{tot}} = -\frac{1}{2}m^*\omega_x^2 x^2 + \frac{1}{2}m^*\omega_y^2 y^2 + \frac{V_0\gamma^2}{\gamma^2 + (x-x_0)^2 + (y-y_0)^2}, \quad (1)$$

where ω_x and ω_y describe the curvature of the saddle-point potential in the x and y directions as extracted from finite-bias measurements at $B = 0$ T [33], V_0 describes the height of the Lorentzian potential, which is proportional to the voltage applied to the tip, and γ denotes the half width at half maximum of the tip-induced potential. If the tip is scanned across the saddle point, the coordinates x_0 and y_0 describe its position.

If the tip is moved close to the QPC, V_{tot} describes a potential landscape, where saddle points that form in between the tip and the QPC walls dominate the current flow. The positions (x_S, y_S) of extremal points of these potentials can be found with the condition

$$\frac{\partial V_{\mathrm{tot}}(x,y)}{\partial x} = \frac{\partial V_{\mathrm{tot}}(x,y)}{\partial y} = 0. \quad (2)$$

Expanding the total potential in a power series around the saddle point found in this way, one obtains

$$V_{\mathrm{tot}} = V_{\mathrm{tot}}(x_S, y_S) + \frac{1}{2}\frac{\partial^2 V_{\mathrm{tot}}}{\partial x^2}\bigg|_{(x_S,y_S)}(x-x_s)^2 + \frac{1}{2}\frac{\partial^2 V_{\mathrm{tot}}}{\partial y^2}\bigg|_{(x_S,y_S)}(y-y_s)^2, \quad (3)$$

with the terms $\frac{\partial^2 V_{\mathrm{tot}}}{\partial x^2}|_{(x_S,y_S)} < 0$ and $\frac{\partial^2 V_{\mathrm{tot}}}{\partial y^2}|_{(x_S,y_S)} > 0$, which can be identified as the shape parameters $-m^*\omega_{xs}$ and $m^*\omega_{ys}$ of the saddle point that is formed in between the tip and the gates. According to Refs. [48,49], only these shape parameters of the potential at the saddle point and the relative position of the potential minimum towards the Fermi energy are needed to calculate the transmission. It has been calculated within the FH model for each position of the tip on a line across the center of the QPC [green line number 2 in Fig. 1(b)]. This model accounts for non-interacting electrons in a potential landscape; however, the included spin splitting uses a g factor that accounts for many particle interactions, as can be estimated from finite-bias measurements in a magnetic field [33].

Additionally, the calculations that follow the CMS model use the electrostatic model developed above to calculate the electrostatic width $2b$ of the channel at the Fermi energy $E_F = 6.7$ meV as a function of tip position. This is the width of the confining parabola in the x direction at E_F. From this width, the electron density in the center of the channel can be estimated to be [47]

$$n = n_0\frac{b}{d}, \quad (4)$$

where d is the lithographic width of the channel of 800 nm and $n_0 = 1.9 \times 10^{11}$ cm^{-2} is taken to be the bulk density

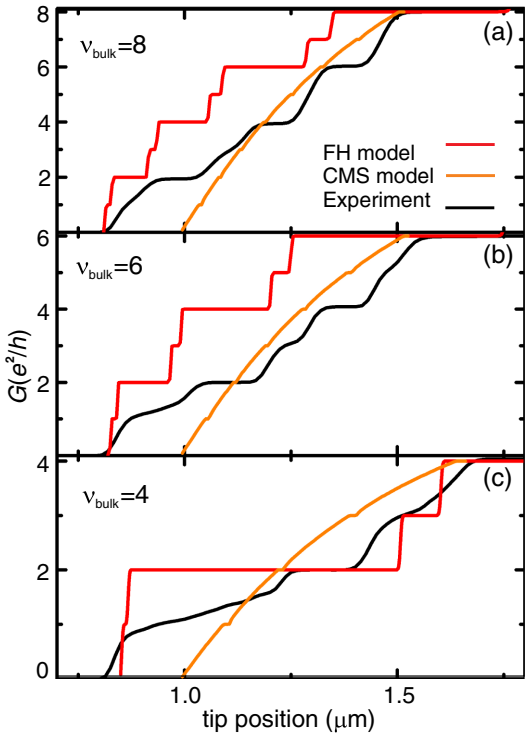

FIG. 5 (color online). Results for bulk filling factors 8, 6, and 4 are shown in (a)–(c), respectively. The black curve corresponds to measured traces at the position of the green line in (a). Red lines and orange lines were obtained by performing calculations according to Refs. [47–49], respectively.

of the 2DEG as determined by quantum Hall effect measurements. Using the channel width and the density in the center of the channel, the transmission can be calculated for each position of the tip across the center of the QPC [green line number 2 in Fig. 1(b)] according to Eqs. (48), (50), and (51) in Ref. [47]. If the tip is placed close to the QPC gap, it is intuitively understandable that the superposition of potentials leads to a modified transmission of current, as the minimum of the confining potential is raised relative to the Fermi energy and the width of the channel is also changed.

In Fig. 5, the results of the FH and CMS models are compared to experimental traces. In both calculations, plateaus can be interpreted as the result of incompressible stripes, while the regions of finite slope represent the compressible stripes in the channel center. One can observe the trend that the calculations that follow the FH model (red curves in Fig. 5) overestimate the plateau width and underestimate the width of the sloped regions, thus giving an exaggerated impression of the incompressible stripe width. On the other hand, the CMS model (orange curves in Fig. 5) overestimates the width of the sloped regions and greatly underestimates the plateau widths, leading to compressible stripes that are broader than those observed experimentally. Our calculations are performed at zero temperature. Including the effect of finite temperature would lead to a stronger smearing of the plateaus. The experiment is found in between the extreme results of the two models. This may not be very surprising. The FH model is based on noninteracting electrons. Self-consistent calculations [8] indicate that edge reconstruction due to screening cannot be neglected in the case of smooth gate-defined edges. However, the CMS model assumes perfect metallic screening by compressible stripes, an assumption that exaggerates the influence of interactions.

V. CONCLUSIONS

In our measurements, scanning gate microscopy has proven to be a powerful tool to explore the integer and fractional quantum Hall effects, adding to conventional transport experiments the possibility to image in real space. Stripes of constant conductance in the maps of conductance as a function of tip position can be identified as the incompressible regions, which form in the center of the constriction in the quantum Hall regime. Their real space and energy distribution can be studied in greater detail. Taking the very local nature of the edge channels into account, it seems surprising that finite-bias spectroscopy measurements show unambiguously that the corresponding energy gaps of incompressible regions of a particular integer filling, here, filling factor 2, do not depend on the position of the tip in the potential landscape. Putting our results in a theoretical context, we can show that existing analytical theories qualitatively reproduce the results but have a tendency to overestimate or underestimate screening effects. Methods such as SGM, which give direct insight into the real-space behavior of electron transport, can connect the theoretical understanding of edge channels to the world of experiments.

ACKNOWLEDGMENTS

The authors acknowledge the Swiss National Science Foundation, which supported this research through the National Centre of Competence in Research "Quantum Science and Technology" and the Marie Curie Initial Training Action (ITN) Q-NET 264034. We thank R. Gaudenzi, Y. Meir, Y. Gefen, M. Büttiker, B. Rosenow, and M. Treffkorn for fruitful discussions.

[1] K. v. Klitzing, G. Dorda, and M. Pepper, *New Method for High-Accuracy Determination of the Fine-Structure Constant Based on Quantized Hall Resistance*, Phys. Rev. Lett. **45**, 494 (1980).

[2] D. C. Tsui, H. L. Stormer, and A. C. Gossard, *Two-Dimensional Magnetotransport in the Extreme Quantum Limit*, Phys. Rev. Lett. **48**, 1559 (1982).

[3] B. I. Halperin, *Quantized Hall Conductance, Current-Carrying Edge States, and the Existence of Extended States in a Two-Dimensional Disordered Potential*, Phys. Rev. B **25**, 2185 (1982).

[4] M. Büttiker, *Absence of Backscattering in the Quantum Hall Effect in Multiprobe Conductors*, Phys. Rev. B **38**, 9375 (1988).

[5] D. B. Chklovskii, B. I. Shklovskii, and L. I. Glazman, *Electrostatics of Edge Channels*, Phys. Rev. B **46**, 4026 (1992).

[6] C. W. J. Beenakker and H. van Houten, in *Semiconductor Heterostructures and Nanostructures*, Solid State Physics, Vol. 44, Henry Ehrenreich and David Turnbull (Academic Press, New York, 1991) pp. 1–228.

[7] J. Dempsey, B. Y. Gelfand, and B. I. Halperin, *Electron-Electron Interactions and Spontaneous Spin Polarization in Quantum Hall Edge States*, Phys. Rev. Lett. **70**, 3639 (1993).

[8] S. Ihnatsenka and I. V. Zozoulenko, *Spatial Spin Polarization and Suppression of Compressible Edge Channels in the Integer Quantum Hall Regime*, Phys. Rev. B **73**, 155314 (2006).

[9] J. Weiss and K. von Klitzing, *Metrology and Microscopic Picture of the Integer Quantum Hall Effect*, Phil. Trans. R. Soc. A **369**, 3954 (2011).

[10] A. M. Chang, *A Unified Transport Theory for the Integral and Fractional Quantum Hall Effects: Phase Boundaries, Edge Currents, and Transmission/Reflection Probabilities*, Solid State Commun. **74**, 871 (1990).

[11] A. H. MacDonald, *Edge States in the Fractional-Quantum-Hall-Effect Regime*, Phys. Rev. Lett. **64**, 220 (1990).

[12] X. G. Wen, *Electrodynamical Properties of Gapless Edge Excitations in the Fractional Quantum Hall States*, Phys. Rev. Lett. **64**, 2206 (1990).

[13] B. Y. Gelfand and B. I. Halperin, *Edge Electrostatics of a Mesa-Etched Sample and Edge-State-to-Bulk Scattering*

Rate in the Fractional Quantum Hall Regime, Phys. Rev. B **49**, 1862 (1994).

[14] C. de C. Chamon and X. G. Wen, *Sharp and Smooth Boundaries of Quantum Hall Liquids*, Phys. Rev. B **49**, 8227 (1994).

[15] X. Wan, K. Yang, and E. H. Rezayi, *Reconstruction of Fractional Quantum Hall Edges*, Phys. Rev. Lett. **88**, 056802 (2002).

[16] K. Yang, *Field Theoretical Description of Quantum Hall Edge Reconstruction*, Phys. Rev. Lett. **91**, 036802 (2003).

[17] R. J. F. van Haren, F. A. P. Blom, and J. H. Wolter, *Direct Observation of Edge Channels in the Integer Quantum Hall Regime*, Phys. Rev. Lett. **74**, 1198 (1995).

[18] R. Knott, W. Dietsche, K. Von Klitzing, K. Eberl, and K. Ploog, *Electro-optic Imaging of Potential Distributions in the Quantum Hall Regime*, Semicond. Sci. Technol. **10**, 117 (1995).

[19] Y. Y. Wei, J. Weis, K. v. Klitzing, and K. Eberl, *Edge Strips in the Quantum Hall Regime Imaged by a Single-Electron Transistor*, Phys. Rev. Lett. **81**, 1674 (1998).

[20] K. L. McCormick, M. T. Woodside, M. Huang, M. Wu, P. L. McEuen, C. Duruoz, and J. S. Harris, *Scanned Potential Microscopy of Edge and Bulk Currents in the Quantum Hall Regime*, Phys. Rev. B **59**, 4654 (1999).

[21] A. Yacoby, H. F. Hess, T. A. Fulton, L. N. Pfeiffer, and K. W. West, *Electrical Imaging of the Quantum Hall State*, Solid State Commun. **111**, 1 (1999).

[22] G. Finkelstein, P. I. Glicofridis, R. C. Ashoori, and M. Shayegan, *Topographic Mapping of the Quantum Hall Liquid Using a Few-Electron Bubble*, Science **289**, 90 (2000).

[23] R. J. Haug, *Edge-State Transport and Its Experimental Consequences in High Magnetic Fields*, Semicond. Sci. Technol. **8**, 131 (1993).

[24] A. M. Chang and J. E. Cunningham, *Transmission and Reflection Probabilities between $\nu = 1$ and $\nu = 2/3$ Quantum Hall Effects and between $\nu = 2/3$ and $\nu = 1/3$ Effects*, Solid State Commun. **72**, 651 (1989).

[25] L. P. Kouwenhoven, B. J. van Wees, N. C. van der Vaart, C. J. P.M. Harmans, C. E. Timmering, and C .T. Foxon, *Selective Population and Detection of Edge Channels in the Fractional Quantum Hall Regime*, Phys. Rev. Lett. **64**, 685 (1990).

[26] B. J. van Wees, E. M. M. Willems, C. J. P. M. Harmans, C. W. J. Beenakker, H. van Houten, J. G. Williamson, C. T. Foxon, and J. J. Harris, *Anomalous Integer Quantum Hall Effect in the Ballistic Regime with Quantum Point Contacts*, Phys. Rev. Lett. **62**, 1181 (1989).

[27] B. R. Snell, P. H. Beton, P. C. Main, A. Neves, J. R. Owers-Bradley, L. Eaves, M. Henini, O. H. Hughes, S. P. Beaumont, and C. D. W. Wilkinson, *Quantised Hall effect and Magnetoresistance Through a Quantum Point Contact*, J. Phys. Condens. Matter **1**, 7499 (1989).

[28] F. P. Milliken, C. P. Umbach, and R. A. Webb, *Indications of a Luttinger Liquid in the Fractional Quantum Hall Regime*, Solid State Commun. **97**, 309 (1996).

[29] D. C. Glattli, H. Rodriguez, V. Perrin, P. Roche, Y. Jin, and B. Etienne, *Shot Noise and the Luttinger Liquid-like Properties of the FQHE*, Physica (Amsterdam) E **6**, 22 (2000).

[30] S. Roddaro, V. Pellegrini, F. Beltram, G. Biasiol, L. Sorba, R. Raimondi, and G. Vignale, *Nonlinear Quasiparticle Tunneling between Fractional Quantum Hall Edge*, Phys. Rev. Lett. **90**, 046805 (2003).

[31] N. Aoki, C. R. da Cunha, R. Akis, D. K. Ferry, and Y. Ochiai, *Imaging of Integer Quantum Hall Edge State in a Quantum Point Contact via Scanning Gate Microscopy*, Phys. Rev. B **72**, 155327 (2005).

[32] N. Paradiso, S. Heun, S. Roddaro, L. Sorba, F. Beltram, G. Biasiol, L. N. Pfeiffer, and K. W. West, *Imaging Fractional Incompressible Stripes in Integer Quantum Hall Systems*, Phys. Rev. Lett. **108**, 246801 (2012).

[33] C. Rössler, S. Baer, E. de Wiljes, P. L. Ardelt, T. Ihn, K. Ensslin, C. Reichl, and W. Wegscheider, *Transport Properties of Clean Quantum Point Contacts*, New J. Phys. **13**, 113006 (2011).

[34] A. E. Gildemeister, T. Ihn, M. Sigrist, K. Ensslin, D. C. Driscoll, and A. C. Gossard, *Measurement of the Tip-Induced Potential in Scanning Gate Experiments*, Phys. Rev. B **75**, 195338 (2007).

[35] N. Paradiso, S. Heun, S. Roddaro, L. N. Pfeiffer, K. W. West, L. Sorba, G. Biasiol, and F. Beltram, *Selective Control of Edge-Channel Trajectories by Scanning Gate Microscopy*, Physica (Amsterdam) E **42**, 1038 (2010).

[36] M. E. Suddards, A. Baumgartner, M. Henini, and C. J. Mellor, *Scanning Capacitance Imaging of Compressible and Incompressible Quantum Hall Effect Edge Strips,* New J. Phys. **14**, 083015 (2012).

[37] V. Venkatachalam, A. Vacoby, L. Pfeiffer, and K. West, *Local Charge of the $\nu = 5/2$ Fractional Quantum Hall State*, Nature (London) **469**, 185 (2011).

[38] A conceptually similar situation arises in the context of *C-V* profiling [50], where a differential measurement of the capacitance versus voltage leads to the extraction of an electron density profile. Even when applied to a quantized system, the results that are based on a classical theory roughly reflect the true quantum-mechanical density distribution (an example is shown in [51]). In analogy, we may roughly (but not strictly) see our dI/dx derivative as a current density profile.

[39] D. B. Chklovskii, *Structure of Fractional Edge States: A Composite-Fermion Approach*, Phys. Rev. B, **51**, 9895 (1995).

[40] C. W. J. Beenakker, *Edge Channels for the Fractional Quantum Hall Effect*, Phys. Rev. Lett. **64**, 216 (1990).

[41] N. Paradiso, S. Heun, S. Roddaro, G. Biasiol, L. Sorba, D. Venturelli, F. Taddei, V. Giovannetti, and F. Beltram, *Imaging Backscattering through Impurity-Induced Antidots in Quantum Hall Constrictions*, Phys. Rev. B **86**, 085326 (2012).

[42] F. Martins, S. Faniel, B. Rosenow, H. Sellier, S. Huant, M. G. Pala, L. Desplanque, X. Wallart, V. Bayot, and B. Hackens, *Coherent Tunnelling across a Quantum Point Contact in the Quantum Hall Regime,* Sci. Rep. **3**, 1416 (2013).

[43] G. A. Steele, R. C. Ashoori, L. N. Pfeiffer, and K. W. West, *Imaging Transport Resonances in the Quantum Hall Effect*, Phys. Rev. Lett.. **95**, 136804 (2005).

[44] L. Cockins, Y. Miyahara, S. D Bennett, A. A. Clerk, S. Studenikin, P. Poole, A. Sachrajda, and P. Grutter, *Energy Levels of Few-Electron Quantum Dots Imaged*

and Characterized by Atomic Force Microscopy, Proc. Natl. Acad. Sci. U.S.A. **107**, 9496 (2010).

[45] R. Willett, J. P. Eisenstein, H. L. Störmer, D. C. Tsui, A. C. Gossard, and J. H. English, *Observation of an Even-Denominator Quantum Number in the Fractional Quantum Hall Effect*, Phys. Rev. Lett. **59**, 1776 (1987).

[46] K.-F. Berggren, G. Roos, and H. van Houten, *Characterization of Very Narrow Quasi-One-Dimensional Quantum Channels,* Phys. Rev. B **37**, 10118 (1988).

[47] D. B. Chklovskii, K. A. Matveev, and B. I. Shklovskii, *Ballistic Conductance of Interacting Electrons in the Quantum Hall Regime*, Phys. Rev. B **47**, 12605 (1993).

[48] H. A. Fertig and B. I. Halperin, *Transmission Coefficient of an Electron through a Saddle-Point Potential in a Magnetic Field*, Phys. Rev. B **36**, 7969 (1987).

[49] M. Büttiker, *Quantized Transmission of a Saddle-Point Constriction*, Phys. Rev. B **41**, 7906 (1990).

[50] J. Hilibrand and R. D. Gold, *Determination of Impurity Distribution in Junction Diodes from Capacitance-Voltage Measurements,* RCA Rev. **21**, 245 (1960).

[51] T. Ihn, K. J. Friedland, R. Hey, and F. Koch, *Magnetotransport Phenomena in Periodically δ-Doped Structures*, Phys. Rev. B **52**, 2789 (1995).